



GelMA/Bioactive Silica Nanocomposite Bioinks for Stem Cell Osteogenic Differentiation

COMPASS

ENGINEERING LIFE GUIDED BY NATURE

This paper must be cited as: Tavares, M. T., Gaspar, V. M., Monteiro, M. V., Farinha, J. P. S., Baleizão, C., & Mano, J. F. GelMA/bioactive silica nanocomposite bioinks for stem cell osteogenic differentiation. *13*(3), 035012. *Biofabrication*, (2021).
<https://doi.org/https://dx.doi.org/10.1088/1758-5090/abdc86>

GelMA/Bioactive Silica Nanocomposite Bioinks for Stem Cell Osteogenic Differentiation

Márcia T. Tavares^{1,2}, Vítor M. Gaspar¹, Maria V. Monteiro¹, José Paulo S. Farinha², Carlos Baleizão², João F. Mano^{1*}

¹CICECO –Aveiro Institute of Materials, Department of Chemistry, University of Aveiro, Aveiro, Portugal

²Centro de Química Estrutural and Department of Chemical Engineering, Instituto Superior Técnico, Universidade de Lisboa, Lisboa, Portugal

Abstract

Leveraging 3D bioprinting for processing stem cell-laden biomaterials has unlocked a tremendous potential for fabricating living 3D constructs for bone tissue engineering. Even though several bioinks developed to date display suitable physicochemical properties for stem cell seeding and proliferation, they generally lack the nanosized minerals present in native bone bioarchitecture. To enable the bottom-up fabrication of biomimetic 3D constructs for bioinstructing stem cells pro-osteogenic differentiation, herein we developed multi-bioactive nanocomposite bioinks that combine the organic and inorganic building blocks of bone. For the organic component gelatin methacrylate (GelMA), a photocrosslinkable denaturated collagen derivative used for 3D bioprinting was selected due to its rheological properties display of cell adhesion moieties to which bone tissue precursors such as human bone marrow derived mesenchymal stem cells (hBM-MSCs) can attach to. The inorganic building block was formulated by incorporating mesoporous silica nanoparticles functionalized with calcium, phosphate and dexamethasone (MSNCaPDex), which previously proven to induce osteogenic differentiation. The newly formulated photocrosslinkable nanocomposite GelMA bioink incorporating MSNCaPDex nanoparticles and laden with hBM-MSCs was successfully processed into a 3D bioprintable construct with structural fidelity and well dispersed nanoparticles throughout the hydrogel matrix. These nanocomposite constructs could induce the deposition of apatite in vitro, thus showing attractive bioactivity properties. Viability and differentiation studies showed that hBM-MSCs remained viable and exhibited osteogenic differentiation biomarkers when incorporated in GelMA/MSNCaPDex constructs and without requiring further biochemical nor mechanical stimuli. Overall, our nanocomposite bioink has demonstrated excellent processability via extrusion bioprinting into osteogenic constructs with potential application in bone tissue repair and regeneration.

Keywords: Silica Nanoparticles, GelMA, 3D bioprinting, Bioinspired, Osteogenic differentiation.

1. Introduction

Bone tissue engineering is receiving an immense interest owing to its potential for providing alternative and more effective bone repair treatments. Presently, autologous, allogenic and synthetic grafts are the most common treatment methodologies, but all have inherent disadvantages that could potentially be overcome through the use of stem cell-laden bioactive hydrogel biomaterials that promote active tissue

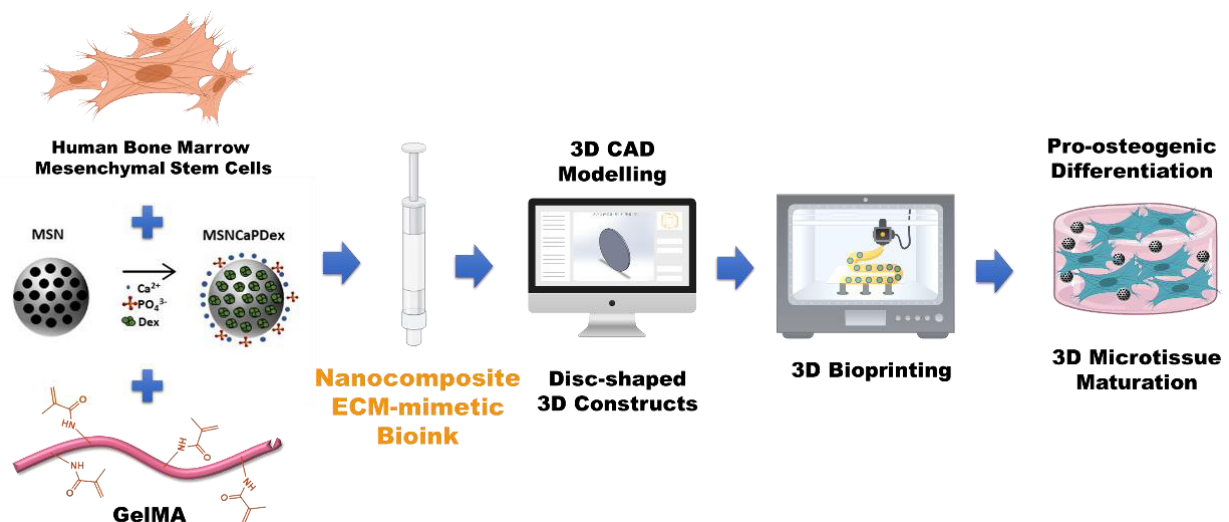


Figure 1 – Mesoporous silica nanoparticles (MSN) are functionalized with calcium and phosphate ions and loaded with dexamethasone (Dex) yielding bioactive MSNCaPDex nanoparticles. These nanocarriers were combined with GelMA and hBM-MSCs to form a nanocomposite bioinstructive bioink. A 3D CAD model was used to design disc-shaped 3D constructs, which were manufactured by 3D bioprinting, as a proof of concept of nanocomposite bioink printability and applicability.

repair through the presentation of multi-dimensional biomolecular cues that stimulate *de novo* bone deposition [1–3]. 3D Bioprinting of [4,5] offers a precise and controlled technique for cell deposition, suitable for the development of anatomically controlled tissue constructs for various biomedical applications [6]. Besides the ability to construct complex structures that mimic bone in composition, 3D bioprinted scaffolds can also be customized to each specific patient bone defect in a personalized medicine approach [7]. The search for superior bioinks to fabricate tailored living implantable constructs for bone tissue repair remains however highly challenging and requires biomaterial combinations exhibiting intrinsic properties for bone progenitor cells adhesion and osteogenic differentiation, while assuring 3D constructs stability and shape fidelity post-printing. From a bottom-up perspective, the hierarchical structure of bone is comprised mainly by a combination of organic and inorganic components, namely nanosized hydroxyapatite crystals and collagen fibers [6,8,9]. Collagen-based hydrogels have been a common choice to recapitulate the organic bone building block owing to their high water content and tunable physicochemical properties and bioactivity [10,11]. Gelatin, a protein derived from the denaturation of collagen, has been extensively explored for this application and also for 3D bioprinting owing to its rheological properties, chemical versatility and inherent bioactivity. One key feature of this biomaterial is the intrinsic presence of cell adhesion motifs such as RGD or matrix metalloproteinases (MMP) cleavable sequences [12,13]. Furthermore, this material exhibits excellent biodegradability, biocompatibility and non-cytotoxicity [14]. By grafting unsaturated methacrylamide groups to gelatin amino/hydroxyl groups, a photocrosslinkable (GelMA) hydrogel that is stable at physiological temperature

(ca. 37 °C) can be obtained, as we and others demonstrated [15–17].

GelMA hydrogels show enhanced mechanical properties, and the chemical modification does impact the exposure of functional groups important for cell attachment. GelMA hydrogels present several advantages for different biomedical applications in tissue repair, from bone, to cardiac [18], muscular [19], cartilage [20] and connective tissue [21]. GelMA from porcine has also been proven to be a suitable bioink for extrusion-based 3D bioprinting, enabling the fabrication of microtissue constructs exhibiting high shape fidelity. Herein, gelatin was selected for the osteogenic bioink formulation due to its correlation with collagen and is aimed to represent the organic component found in the native bone tissue. Nevertheless, GelMA presents some challenges regarding the optimization of its printability window, namely regarding final concentration and possible spontaneous crosslinking, especially with porcine gelatin [22–24].

Aiming to include the nano building blocks found in native bone tissues, attempts to use nanocomposite biomaterials have also been reported in the context of bone tissue repair [6,8,9,25]. Bioactive silica nanoparticles have shown to be particularly attractive as they can be leveraged for inducing hydroxyapatite formation and to bioinstruct stem cells toward osteogenic lineages by releasing inorganic ions including calcium, phosphate and silicate, or stem cell bioinstructive drugs, as we and others demonstrated [26–29]. Moreover, nanosilicates are recognized to provide enhanced physical, chemical, and biological functionality to different types of materials [27,30,31]. Particularly, mesoporous silica nanoparticles (MSNs) have been commonly employed as nanocarriers due to their mesoporous structure that allows bioactive molecules loading, high surface-to-volume ratio,

and chemical versatility that allows its straightforward surface functionalization with a number of moieties [32]. Calcium and phosphate ions, which positively influence stem cells osteogenic differentiation, bone matrix deposition and mineralization, [33] have been integrated in MSNs to form bioactive glass nanospheres [34]. Dexamethasone (Dex), a glucocorticoid known to induce osteogenesis [35,36], was also incorporated in MSN nanoparticle pores to obtain bioinstructive systems that exhibit osteoconductive osteogenic differentiation properties [34]. Recently, we synthesized multifunctional MSNs nanocarriers incorporating Dex and pro-osteogenic minerals (MSNCaPDex) [37]. Such multifaceted carriers were able to promote stem cells osteogenic differentiation in a single administration.

Herein we report the design of a 3D bioactive bioink that combines MSNCaPDex nanoparticles and GelMA hydrogels laden with hBM-MSCs, as illustrated in figure 1. This approach recapitulates the major inorganic/organic components of bone matrix (GelMA -organic component; MSNCaPDex nanoparticles - inorganic nanosized components), and also key cellular constituents that are recognized to differentiate into bone cells under specific conditions and to contribute for bone tissue deposition. The nanocomposite biomimetic bioink composition was optimized for enabling 3D extrusion bioprinting of disk-shaped hBM-MSCs laden constructs as a proof of concept. Initially an optimization of 3D bioprinting parameters including printing pressure and GelMA incubation on ice were optimized, to maximize the 3D printed constructs shape fidelity post printing. Stem cell viability and osteogenic differentiation was evaluated post-printing. The newly formulated nanocomposite bioink shows great potential for being used in bone tissue engineering applications.

2. Experimental Section

2.1 Materials

Tetraethylorthosilicate (TEOS, 98%), N-cetyltrimethylammonium bromide (CTAB, 99%), sodium hydroxide solution (25 % NaOH), absolute ethanol (99.9%), calcium hydroxide (≥ 95 %, $\text{Ca}(\text{OH})_2$), ammonium hydrogen phosphate (98%, DHP), Gelatin Type A from porcine skin, Irgacure 2959 and p-Nitrophenyl phosphate were acquired from Merk-Sigma (Sintra, Portugal). Glycidyl methacrylate (97%) were obtained from ACROS organics. All of the following cell culture media and supplements namely GIBCO Dulbecco's Phosphate buffered saline (DPBS), Fetal Bovine Serum (FBS; E.U. approved, South America origin), TrypLETM Express, GIBCO[®] Antibiotic/antimycotic solution (ATB) containing 10,000 units/mL of penicillin, 10,000 mg. mL⁻¹ of streptomycin, and 25 mg. mL⁻¹ of Gibco Amphotericin B were purchased from ThermoFisher Scientific (Alfagene, Portugal). Trypsin was obtained from

Sigma-Aldrich (Germany). Ultra-Low-Adhesion (ULA) round-bottom 96-wells plates were purchased from Corning (Corning, NY, US). Calcein-AM, Propidium Iodide (PI) and b-Glycerol phosphate were all purchased from Thermo Fisher Scientific Inc (Alfagene, Carcavelos, Portugal). Alizarin Red S was obtained from Laborspirit (Loures, Portugal). To visualize MSNCaPDex nanoparticles dispersion in the bioprinted 3D hydrogel matrix, a fluorescent molecule (perylene diimide-PDI) was incorporated in nanoparticles structure, as reported elsewhere [38].

2.2 Synthesis of Bioactive Mesoporous Silica Nanoparticles

The preparation of MSNs was based on a previously described procedure [39,40]. Briefly, in a polypropylene flask, 240 mL of MilliQ water was mixed with 1.75 mL of NaOH (1.7 M) at 40 °C. Once the temperature was stabilized, 0.5 g of CTAB was added. After 30 min, 2.5 mL of TEOS was added dropwise while stirring. The reaction was then left to proceed for 2 h. After cooling at RT, the dispersion was centrifuged (30,000 g, 20 min) and washed three times with a mixture of ethanol/water (50 % v/v). The resulting particles were dried at 50 °C in a ventilated oven.

For the addition of calcium and phosphate ions [29,37], MSNs were initially dispersed in milli-Q water. After, calcium hydroxide ($\text{Ca}(\text{OH})_2$) and diammonium hydrogen phosphate ($(\text{NH}_4)_2\text{HPO}_4$, DHP) solutions were added directly into the dispersion at a concentration of 0.15 g L⁻¹ and 0.10 g L⁻¹ respectively. The mixture was left stirring overnight at room temperature. For recovery, the dispersion was centrifuged and MSNCaP (MSN particles functionalized with calcium and phosphate) were washed 3 times with milli-Q water and dried at 50 °C. To remove the template, the particles were calcinated at 550 °C for 6 h.

Dexamethasone (Dex) was incorporated in the pore structure by combining 100 mg of MSNCaP and 4 mg of Dex in 0.4 mL of ethanol. The mixture was stirred for 24 h, at RT. The drug loaded nanoparticles were collected by centrifugation, washed with TRIS-buffer solution (10 mM TRIS, 0.17M NaCl, pH=7.4) three times and dried at RT.

2.3 Synthesis of Methacrylated Gelatin

Porcine gelatin type A was chemically modified with methacryloyl functional moieties as we previously described [17]. Initially, a 10 % (w/v) gelatin solution was prepared by dissolving gelatin in PBS (pH=7.4), under vigorous magnetic stirring, at 50 °C, overnight. Methacrylic anhydride (0.6 g / g of gelatin) was added slowly to the mixture and the reaction was left for 5 h, at RT. The chemically modified gelatin was centrifuged at 3500 g for 3 min at RT to remove the unreacted methacrylic anhydride. The GelMA containing supernatant was diluted with 10 mL of deionized water and transferred to

a regenerated cellulose dialysis membrane (MWCO 6-8 kDa). GelMA was dialyzed at 50 °C against deionized water for 5-7 days protected from light. The purified methacrylated polymer was freeze dried. The degree of substitution (ca. 89 %) was determined according to previously established procedures [17].

2.4 3D Bioprinting of Nanocomposite GelMA hydrogels

Extrusion based printing was performed using an Inkredible + 3D bioprinter (CELLINK, Germany). The CAD models were designed in SolidWorks® (Dassault Systems SA). The files were imported into CELLINK Heartware software and post processed with Slic3r (v 1.3.0) to obtain g-code files with specified layer patterns, infills and print speeds suitable for the CELLINK Inkredible + Bioprinter. Printability test was performed using inks without cells and printed, first onto petri dishes and, subsequently the g-code was reprogrammed to print these models on 12-well culture plates. Previous to any printing, GelMA bioinks (10 % w/v) containing Irgacure 2959 (0.1 % w/v) were prepared and maintained at 37 °C. Before the bioprinting process the bioinks remained on ice for different time windows (figure 2). Nanocomposite bioinks comprised GelMA (10 % w/v), 0.5 % MSNCaPDex and the photoinitiator (Irgacure 2959, 0.1 % in PBS pH=7.4). 3D disk shaped constructs were printed at a speed of 10 mm s⁻¹, with a 23G nozzle (blunt needle - 0.33 mm inner diameter, CELLINK, Germany), at different pressures. All the printing stages were performed in a printing bead at RT and the print head temperature was maintained between 20-21 °C, at all times. Temperature-dependent printability window was determined in the equipment printhead (T = 20-21°C) by using a thermocouple probe (Type K thermocouple, laser thermometer RayTemp® 8) inserted inside the printing cartridge to be in contact with the bioink. Constructs were initially 3D printed in petri dishes with 70 % infill and then in 12 well plates with 100 % infill density using the Archimedean chords slicer pattern. All the 3D bioprinted structures were posteriorly crosslinked by using a U.V. light for 5 min, at RT (Omniscure S2000, 0.86 W/cm²).

Fillament collapse test was performed as described in the literature [40]. In brief, the mid-span deflection of the 3D bioprinted fillament was accessed in a 3D printed platform (Black PETG part with the following dimensions: l x w x h = 2.0 x 2.0 x 4.0 mm, HelloBee Prusa 3D Printer), with precisely spaced pillars (1.0, 2.0, 4.0, 8.0 and 16 mm spacing). The fillament deposition was performed by using a g-code obtained from [41]. The printing parameters were as above mentioned and the nozzle tip was set at 0.3 mm gap above the top of the pillars.

Fillaments fusion test was performed as described in the literature, with slight modifications [41]. In brief, 3D printed GelMa/ MSNCaPDex nanocomposite bioinks were printed at a constant speed of 10 mm .s⁻¹, using a pattern starting at 0.25

mm and ending at 0.55 mm distance. Digital photographs were acquired (CANON EOS, Macro lens) after printing and U.V. mediated crosslinking.

2.5 In vitro bioactivity study

In vitro bioactivity tests were carried out at 37 °C under orbital shaking (50 rpm) in simulated body fluid (SBF). The preparation of SBF followed the protocol described by Kokubo and colleagues [42]. For this evaluation, each hydrogel was immersed in 20 mL of SBF for 1 and 3 days. After removing SBF, the samples were rinsed with distilled water and freeze dried (-86°C, LyoQuest, Telstar). The samples were then analyzed by using Attenuated Total Reflectance-Fourier transform infrared spectroscopy (ATR-FTIR, Bruker Alpha, controlled by the OPUS software v7.0) and powder X-ray diffraction (XRD, D8 Advance Bruker AXS θ -2 θ diffractometer, equipped with a copper radiation source (CuK α , λ =1.5406 Å) and by scanning electron microscopy coupled with energy dispersive spectroscopy (SEM-EDS, Hitachi SU-70, operating voltage 15 kV).

2.6 In vitro cell culture-hBM-MSCs encapsulation

Human bone marrow mesenchymal stem cells (hBM-MSCs, ATCC® PCS-500-012™) were cultured in basal medium (α -MEM, 10 % FBS and 1 % penicillin-streptomycin) and were left to adhere and proliferate for 3 days. hBM-MSCs were used until passage 6. Cell suspension was routinely prepared by trypsinization with TripeLE® Express. The cells were incorporated into GelMA solutions at a final density of 4x10⁶ cells mL⁻¹ and were further incubated for 1, 7, 14 and 21 days post 3D bioprinting. For cell characterization studies, sterilized MSNCaPDex nanoparticles (washed in ethanol for 2 h) were added to the GelMA solution to formulate the nanocomposite bioink. Each time point had a negative control (basal medium) and a positive control (osteogenic medium - basal medium supplemented with ascorbic acid (10 x 10⁻³ M), Dexamethasone (Dex - 100 x 10⁻⁹ M) and β -glycerophosphate (50 μ g mL⁻¹), both conditions were devoid of MSNCaPDex nanoparticles.

2.7 Live/Dead assay

At predetermined time points, hydrogels were incubated in a solution of 2 μ L of calcein-AM (4x10⁻³ M solution in DMSO) and 1 μ L of propidium iodide (1 mg mL⁻¹ in 1000 μ L of PBS) at 37 °C, during 30 min. After washing with PBS, hydrogels were examined using an upright fluorescence microscope (Zeiss Imager M2) equipped with a monochromatic CCD camera (AxioCam, 3Mpix). Image processing was performed by using the ZEN v2.3 blue edition software (Carl Zeiss, Oberkochen, Germany).

2.8 Metabolic Activity

The effect of different nanoparticle formulations on the metabolic activity of hBM-MSCs was investigated by using the alamarBlue[®] assay (Invitrogen). For these assays, alamarBlue[®] was incubated in culture medium at a 1:10 ratio, according to the manufacturer's instruction. Throughout the assay the cells were incubated at 37 °C, in 5 % CO₂, for 6 h. After incubation, the medium from each well was transferred to black-well clear bottom 96-well plates (SPL Life Sciences). Fluorescence of the resorufin product was then measured by using a multimode microplate reader (Biotek Synergy HTX) equipped with a $\lambda=540/35$ nm band-pass excitation filter and a $\lambda=600/40$ nm band-pass emission filter.

2.9 Cell proliferation by DNA Quantification

Double-strained DNA (dsDNA) quantification assay (PicoGreen[®], ThermoFisher Scientific) was performed to evaluate cell proliferation. In specific time points, the culture media was removed, and the 3D bioprinted hydrogel was washed with PBS. Sterilized water was added to the cells, which were afterwards frozen at -80 °C. The samples were thawed and sonicated for 30 min to induce complete membrane disruption. Supernatant fluorescence was measured ($\lambda=485/20$ nm excitation and $\lambda=528/20$ nm emission) in a multi-modal microplate reader (Synergy HTX, BioTek Instruments, USA). DNA amount was then calculated by resorting to a standard curve ranging from 0 to 1 $\mu\text{g mL}^{-1}$.

2.10 Osteocalcin and bone morphogenic protein 2 quantification

The amount of osteocalcin (OCN) and bone morphogenic protein 2 (BMP-2) secreted by cells laden in the 3D constructs was assessed by ELISA. For this, cell culture media was retrieved at 21 days of culture and stored at -80 °C until analysis. Commercially available ELISA kits: (i) Human OCN (ab270202, Abcam, UK) and (ii) Human BMP-2 (EHBMP2, Thermo Fisher Scientific, Alfagene, Portugal) were used for this quantification and the procedures used were according to the manufacturer's recommendations. The samples absorbance was analysed at $\lambda = 450$ nm in a multi-mode microplate reader (Synergy HTX, BioTek Instruments).

2.11 Hydroxyapatite Fluorescence Staining

Hydroxyapatite crystals were assessed using the OsteoImage[™] Mineralization Assay kit (Lonza) according to the manufacturer's instructions. Samples were counterstained with DAPI (1:1000 in PBS, 1 mg mL⁻¹, ThermoFisher Scientific) for 5 min at RT. The images were acquired using a Stemi 508 Stereo Microscope (Carl Zeiss, Oberkochen, Germany).

2.12 Alizarin Red S Mineralization Assay

Hydrogels were fixed and washed as previously mentioned, and incubated with 1 mL of Alizarin Red S (4×10^{-4} M, pH=4.2), for 1h, at RT. The staining solution was then removed, and the cells rinsed three times with PBS (pH=7.4). The images were acquired using a Stemi 508 Stereo Microscope (Carl Zeiss Oberkochen, Germany).

2.13 Statistical Analysis

Data are presented as mean \pm standard deviation in each experiment. The statistical analysis was performed by using the one-way ANOVA with post hoc Tukey's multiple comparisons tests, using GraphPad Prism v6.00 software (San Diego, USA). Statistical significance was defined at $p < 0.05$ for a 95% confidence interval.

3. Results and Discussion

3.1. Fabrication of GelMA- MSN/CaPDex organic-inorganic hydrogel constructs

Herein, we report the formulation of a bioinspired and biomimetic nanocomposite 3D bioink comprising both organic and inorganic components, recapitulating the composite nature of native bone, with potential to support stem cell adhesion and autonomously promote pro-osteogenic differentiation without the addition of further stimuli. To materialize this concept, multifunctional MSNs containing calcium, phosphate and dexamethasone (MSN/CaPDex) were synthesized following previously optimized procedures, resulting in nanoparticles with a diameter of 63 ± 8 nm (figure 2) [37]. The dexamethasone release, bioactivity and also ions release has been previously analysed and validated [29,37]. Such nanoparticles constituted the inorganic building blocks. Afterwards, to modulate the organic elements, gelatin was chemically modified with methacrylate groups as we have previously described, resulting in a GelMA photocrosslinkable derivative [17]. After synthesizing the two key inorganic/organic components of the bioink, the first challenge was to bioprint stable 3D constructs using GelMA. For the proof of concept, all the constructs were printed in disk form (designed using CAD models, figure 3A) via the

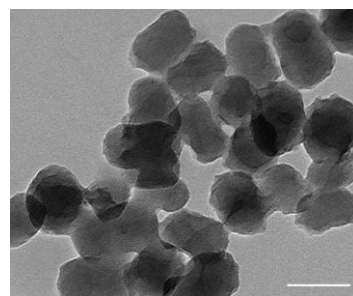


Figure 2 – TEM micrograph of MSN/CaPDex nanoparticles (scale bar = 100 nm).

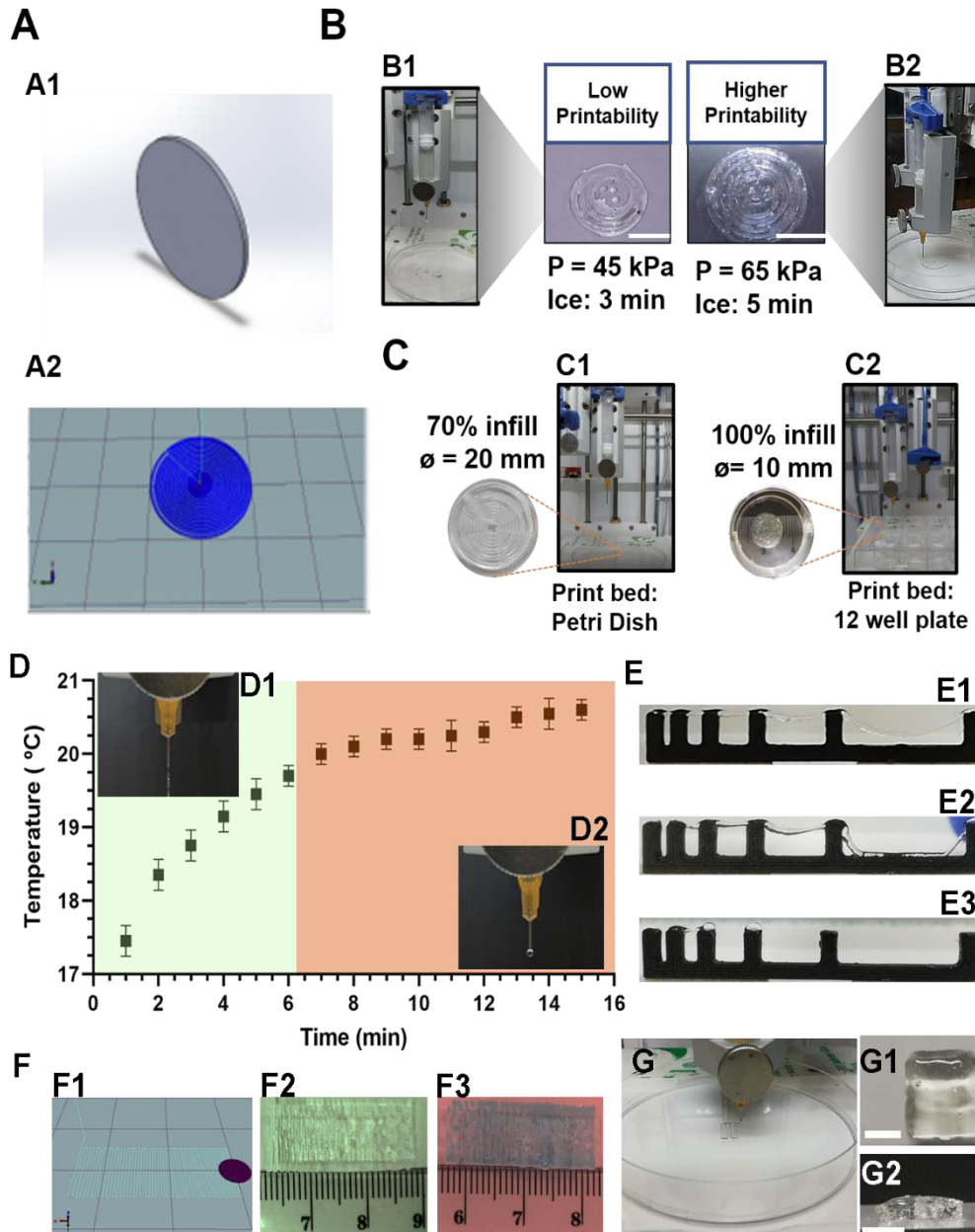


Figure 3 – 3D printing process of GelMA-based constructs. (A) Computer aided designed disk part produced using (A1) Solid Works software and post-processed in (A2) CELLINK Heartware - Slic3r, prior to printing. (B) Effect of low temperature incubation in GelMA 10% formulations processing and printability using the 23G nozzle. (B1) While 3 min in ice yielded shapeless constructs. (B2) 5 min incubation, and printing at a pressure of 65 kPa led to a higher printability. Scale bar = 1 cm. (C) 3D bioprinting of different sized disks using different infill parameters. (C1) In the larger disk a 70 % infill renders, while with (C2) 100% infill forms smaller disks. (D) Analysis of GelMA/MSNCaPDex bioink printing window as a function of temperature. Green box - Optimal printing window; Faint red box – Sub-optimal and dripping regime for the GelMA/MSNCaPDex. (D1) Nanocomposite GelMA/MSNCaPDex nanocomposite bioink extruded into a uniform fillament within the optimal printing window (time out of ice incubation: 0:00 ~ 6:00 min, at printhead temperature setting: 21 °C). (D2) Dripping regime and no apparent fillement formation. (E) Fillament collapse test for GelMA/MSNCaPDex nanocomposite bioink. (E1) Bioink fillament collapse within the optimal printing window. (E2) Bioink fillament collapse at the end of the optimal printing window, ca. 6 min. (E3) Dripping regime - no fillament formation. (F) Fillament fusion test for the GelMA/MSNCaPDex nanocomposite bioink. (F1) 3D CAD design for fillament fusion test. (F2) Fillament fusion for GelMA/MSNCaPDex bioink extruded within the optimal printing window ($t = [0\sim6 \text{ min}]$). (F3) Fillament fusion for GelMA/MSNCaPDex bioink. (G) 3D printed 3 layer cube shaped construct with GelMA/MSNCaPDex nanocomposite bioink to evaluate the printability of multiple layers withing the optimal printing window. The beginning of the bioprinting process is demonstrated. Fillament strand distance: 0.61 mm. (G1 and G2) Representative digital photograph of printed constructs, top and laterall view, respectively. Scale bar = 0.5cm.

deposition of a spiral pattern. Viscosity is an important parameter to take into consideration when 3D bioprinting an hydrogel bioink comprised by GelMA via extrusion bioprinting. Generally, relatively high concentrations of GelMA are required to avoid compromising the printability and the fidelity of the final 3D construct [22]. Herein, the bioink was formulated with 10 % GelMA, a value reported to upkeep cell viability post-crosslinking [14,16]. GelMA is a temperature-sensitive biomaterial, in liquid form at 37 °C and exhibiting high viscosity at lower temperatures. For 3D bioprinting, an equilibrium between viscosity and flowability must be identified for each extrusion bioprinter system/equipment in order to print a stable construct, without clogging the nozzle or causing dipping during printing [15]. As represented in figure 3B, several parameters were tested to optimize the bioprinting process, including the temperature of the bioink. Herein GelMA solutions were prepared at 37 °C

and allowed to cool down to increase viscosity before bioprinting, as reported in different studies and manufacturer protocols [22,24,43]. However, such protocols are generally poorly defined and therefore we optimized a protocol for GelMA (10%, in PBS pH =7.4) cooling by incubation on ice for different time periods and evaluated its printability. The incubation time GelMA was crucial to attain the proper viscosity for extrusion bioprinting in the CELLINK Inkredible + 3D Bioprinter equipped with a standard 3 mL printing cartridge and a 23G nozzle. Three main parameters were manipulated during the printing process optimization: (i) the printing pressure and (ii) the cooling time. All the other parameters including printing speed (10 mm s^{-1}), fill pattern (Archimedean chords) and layer height were maintained constant. While poorly defined filaments and shapeless constructs were obtained following GelMA incubation on ice for 3 min (figure 3B1) (45 kPa), upon increasing the

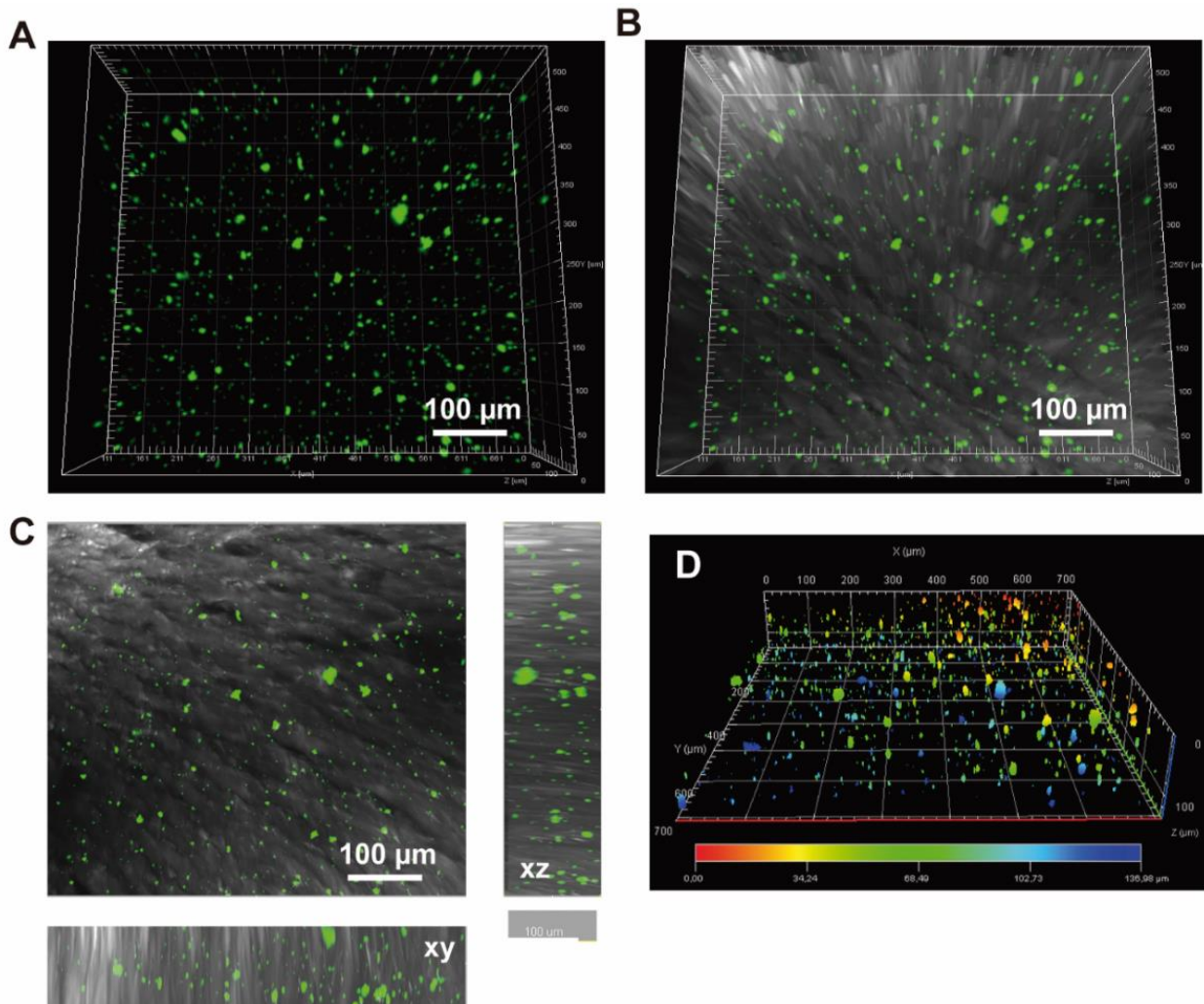


Figure 4- Nanoparticles dispersion in nanocomposite constructs obtained by CLSM imaging. 3D reconstruction showing the MSNCaPDex in the GelMA hydrogel: (A) fluorescence micrographs. (B) brightfield and fluorescence micrographs. (C) Extended orthogonal projection with the corresponding yz and xz 3D orthogonal projections. (D) Depth-coding 3D reconstruction image displaying MSNCaPDex dispersion at various depths in the GelMA 3D hydrogel construct, post-printing.

incubation time up to 5 min (figure 3 B2), a construct with a highly defined shape was obtained (figure 3B2). Conversely, when extruding viscous GelMA formulations, a higher pressure was required to maintain filament extrusion and consequently a shape-defined 3D construct.

The infill density for this particular geometry and disk sizes were also investigated (figure 3C). The 3D printing of disks with 20 mm diameter was initially performed by using a petri dish as a printing bed (figure 3C1, 20 mm constructs). The 3D printing of various 10 mm constructs in a 12-well plate was also evaluated. This allowed to increase the manufacturing speed and number of cell-laden constructs printed in a single run, thus reducing the time that stem cells were maintained outside optimal culture conditions. The fact that it is possible to bioprint constructs in individual wells allows for possible high-content experiments that require multiple structures [30]. For the following experiments, 10 mm constructs bioprinted with an infill of 100 % were employed (figure 3C2). The fabrication of such 3D constructs was only possible by

determining the optimal printing window for the GelMA/MSNCaPDex formulation. As previously mentioned this ink is temperature sensitive and thus determining the temperature-dependent printing window where a stable filament can be extruded is crucial. Similar to the cooling time, also the printing window for GelMa-based bioinks is generally poorly defined. Hence, to better characterize the printability window for the newly formulated ink we recorded in real time the temperature in the printing cartridge after loading into the printhead. As shown in figure 3D the printing window post removal of the cartridge from the ice is rather narrow ($t = 0-6$ min). In this window, a stable and well defined filament was extrudable (figure 3D1), as also demonstrated by the filament fusion and filament collapse test (figure 3E and F). Particularly, it was clear that in the printing window the extruded filaments are able to bridge the largest distance between pillars (16 mm), although it is important to mention that filament sagging was observed even in the optimal window (figure 3E1 and E2). Also, in the printing window

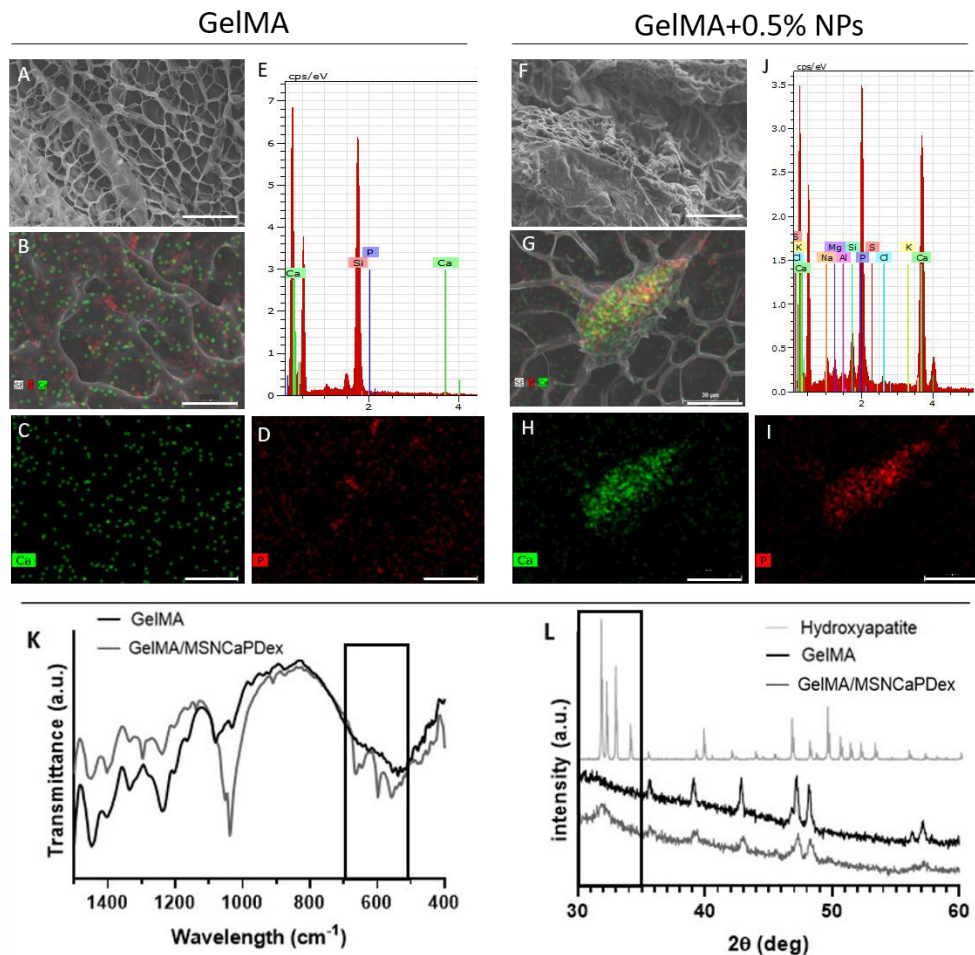


Figure 5 - Mineralization in GelMA and GelMA/MSNCaPDex hydrogels immersed in SBF for 3 days. (A, F) Scanning electron microscopy (SEM) micrographs (scale bar = 100 μ m), and (B-D, G-I) EDS mapping showing silica, calcium and phosphorous ions presence in the hydrogel matrix (scale bar = 30 μ m). (E, J) EDS spectra. (K) Fourier- Transform Infra-Red (FTIR) spectra and (L) powder X-ray diffraction data.

some filament fusion was observed, this could be partially due to the selected nozzle and to the distance in the last strands (0.55 mm). In fact, when a larger strand-to-strand distance was used no fusion was observed (figure 3G). Under optimal conditions the GelMA/MSNCaPDex formulation was able to be used also for fabricating 3-layered cube shaped constructs (figure 3G1 and G2). Interestingly past the printing window a dripping regime was obtained as observed by the droplets in the filament collapse test and also by the incomplete strands of the filament fusion analysis (figure 3E and F). This indicates the importance of characterizing these parameters when designing new nanocomposite bioinks based on thermosensitive GelMA biomaterials.

After optimizing the 3D printing with GelMA alone, 0.5 % of MSNCaPDex and hBM-MSCs were incorporated to generate the nanocomposite bioink. During the optimization stages, it was observed that a MSNCaPDex nanoparticle concentration of 1% w/v was difficult to properly homogenize in GelMA hydrogel. Hence, a final concentration of 0.5 % w/v was used to obtain printable nanocomposite constructs. This nanoparticle amount is comparable to that employed in other exploring the formulation of MSN biomaterial inks [44]. In all experiments, hBM-MSCs - GelMA hydrogel bioinks containing only the organic bone component and the bone progenitor cells were used as a control.

Nanoparticles dispersion within the 3D printed hydrogel matrix was observed by confocal laser scanning microscopy (figure 4). The 3D image reconstruction obtained from single z-stacks (figure 4A/B) and the orthogonal projection (figure 4C) show that MSNCaPDex nanoparticles are well dispersed throughout the hydrogel matrix volume. A few particle aggregates are observed, possibly formed due to colloidal destabilization by the PBS present in the GelMA solution.

3.2 In Vitro Bioactivity Studies

The presence of bioactive nanoparticles in 3D bioprinted hydrogel constructs can positively impact material's bioactivity and stem cell bioconstructive properties due to the release of calcium, phosphate and silicate ions [45]. Such inorganic mediators are widely recognized to be involved in bone repair process. MSNCaP nanoparticles proved to have *in vitro* bioactivity when submerged in simulated body fluid (SBF) [37]. The bioactivity of the nanocomposite hydrogels was also assessed by performing *in vitro* studies using SBF. This experimental design was employed owing to its previous validation [46] regarding the value of including dexamethasone and of the release of the ions from the MSNCaPDex nanoparticles, leading to a synergistic pro-osteogenic effect in MSCs, as we have previously observed [37]. The differences between GelMA and GelMA/MSNCaPDex after 3 days in SBF, can be observed in figure 5. Even though the porous network is still visible in both hydrogels (figure 5 A/F), in GelMA/MSNCaPDex, the

presence of calcium/phosphate bone-like apatite is clear as demonstrated by EDS mapping (figure 5 G/H/I) and EDS spectrum (figure 5 J). The obtained Ca/P ratio of 1.72, is close to the generally assigned to the presence of calcium phosphate mineral-like apatite [47]. Further presence of hydroxyapatite will be further addressed in the following assays using hydroxyapatite specific labelling agents. In control hydrogels, traces of calcium and phosphorous were observed in the nanocomposite hydrogel (figure 5 B/C/D), probably due to salt deposition from the SBF (the EDS spectra exhibits other elements present in SBF in the same proportion as calcium and phosphorous, figure 5E). Furthermore, SEM micrographs (figure 5B) indicate that no structure resembling apatite was formed in the control formulations.

The bioactivity of the MSNCaPDex present in the nanocomposite hydrogel was confirmed by Fourier transform infra-red spectroscopy (FTIR) (figure 5K) and by X-ray diffraction (XRD) (figure 5L). The GelMA/MSNCaPDex FTIR spectra exhibits the stretching vibration peaks characteristic of phosphate groups (600 cm^{-1} , 580 cm^{-1} , 1100 cm^{-1}), as well as a peak at ca. 1000 cm^{-1} , assigned to the Si-O-Si asymmetric stretching mode of the silica nanoparticles [48]. The XRD diffractogram of the GelMA/MSNCaPDex nanocomposite hydrogels demonstrates a peak at ca. 30° that may be assigned to hydroxyapatite [49]. However, to further corroborate the presence of hydroxyapatite portion of bone-like nodules deposited by cells additional assays were executed as it will be demonstrated in figure 7.

These results indicate that the single incorporation of 0.5 % w/v MSNCaPDex nanoparticles in the GelMA hydrogel matrix is suitable to impart a bioactive profile after 3 days in contact with SBF. Although in previous studies bioactive GelMA hydrogels were obtained by incorporating silica nanoparticles [50] or bioactive glass nanoparticles [51], significantly higher concentrations were required (1.6 wt% and 2.5 wt% respectively), and the silica nanomaterials used were non-porous and did not present the multi-functionality of MSNCaPDex nanocarriers. The nanoparticles used herein included two relevant features as they: (i) incorporate inorganic components that could be released faster than in compact objects due to their mesoporous nature; and (ii) have the possibility to be loaded with stem cell bioconstructive molecules (e.g. Dex, Naringin) that are critical for stem cells pro-osteogenic differentiation [52].

3.3 Cell viability

To assess stem cells viability in the 3D bioprinted nanocomposite hydrogel, the metabolic activity was normalized using the GelMA-3D bioencapsulated cells that were in contact with basal medium (figure 6A). The DNA content was quantified for all the experiments to evaluate hBM-MSCs proliferation throughout the time frame of the study (figure 6B). Stem cells metabolic activity and DNA

content in all conditions tested remained similar throughout the 21 days of culture. The metabolic activity data indicates that stem cells remain viable in the constructs. Interestingly, the DNA content does not significantly increase during the time frame, indicating that cells are not very actively proliferating, such is generally correlated to the fact upon activating the differentiating intracellular pathways stem cells proliferation rate decreases, as we and others have observed [53]. Complementary, live/dead assays were performed after 1, 7 and 14 days. As demonstrated by fluorescence micrographs, hBM-MSCs cells remained viable 1-day post bioprinting and even after 2 weeks of culture (figure 6C). These results indicate that neither the 3D bioprinting process

(BMP-2) and osteocalcin (OCN) are key bone biomarkers that are known to be involved in bone formation and matrix deposition [52,54]. BMP-2 ELISA-mediated quantification evidences that cells encapsulated in nanofunctionalized hydrogels had a higher pro-osteogenic response when compared with the other conditions, especially when compared to the basal medium (figure 7B). After 14 days the levels of BMP-2 are significantly higher for hBM-MSCs incubated in the presence of MSN/CaPDex when compared to both controls. After 21 days, the BMP-2 level in the pro-osteogenic medium positive control is similar to that of the 3D bioprinted nanocomposite. Concerning the OCN biomarker, pro-osteogenic medium and nanocomposite hydrogels

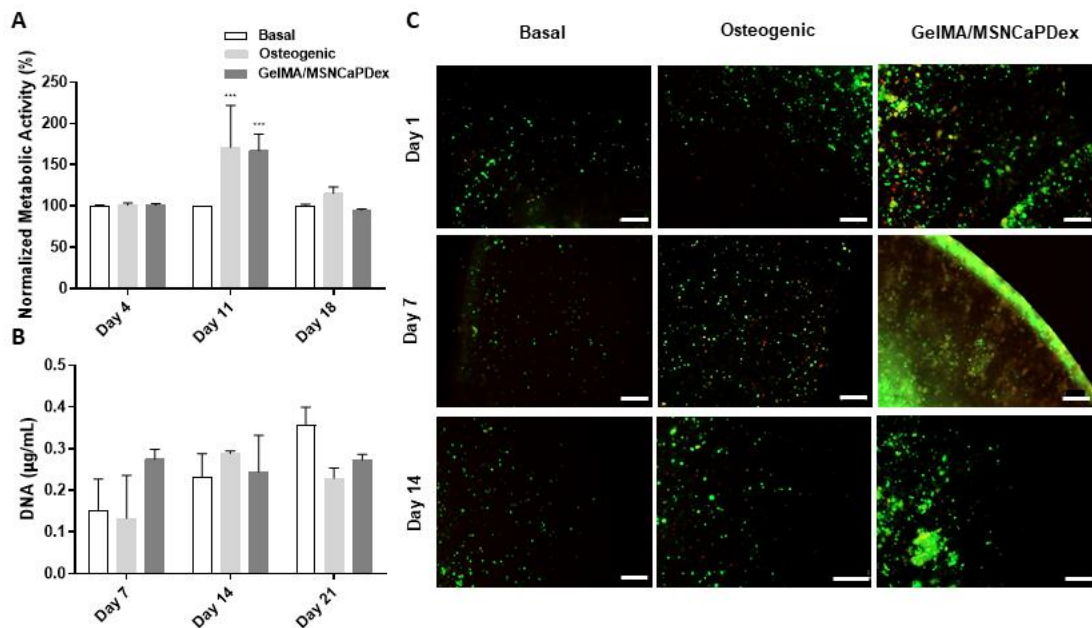


Figure 6 – Analysis of GelMA/MSN/CaPDex cell laden constructs potential for guiding stem cells osteogenic differentiation. (A) Normalized Metabolic Activity, (B) hBM-MSCs DNA quantification. (C) Live/dead assays of encapsulated hBM-MSCs in standard GelMA hydrogels and and 0.5 % GelMA/MSN/CaPDex nanocomposite 3D bioprinted constructs at different time points (1, 7 and 14 days). Scale bar = 200 µm. Data represents mean ± s.d., n=3, ***p<0.001.

nor the encapsulation in GelMA affected hBM-MSCs viability [22,55,56].

3.4 Osteogenic Differentiation

We hypothesise that MSN/CaPDex nanoparticles are able to release bioinstructive bioactive factors within the 3D bioprinted hydrogel matrix to induce hBM-MSCs pro-osteogenic differentiation. The differentiation study consisted of three different experimental groups: The positive and negative control (GelMA 3D constructs in basal and osteogenic medium, respectively) and the nanocomposite GelMA/MSN/CaPDex hydrogel (figure 7A). To assess stem cells response upon contact with the bioinstructive bioactive factors of MSN/CaPDex nanoparticles, key osteogenic biomarkers were evaluated. Bone morphogenetic protein

exhibited similar levels, and higher than those of the basal medium (figure 7C). One important feature of osteogenically differentiated cells is their role in mediating the formation of calcium nodes and hydroxyapatite, both related with cell-induced mineralization. As expected, the absence of hydroxyapatite is clear when cells are incubated in basal medium. Whereas when cells are in contact with either osteogenic medium or the GelMA/MSN/CaPDex nanocomposite hydrogels a clear green signal (OsteoImager™ signal for hydroxyapatite presence) is obtained. As demonstrated in figure 7D hydroxyapatite staining (Green spots) can be observed. The same behavior is observed in the Alizarin Red S staining, with the calcium nodes being easily identifiable. The fact that cell mineralization is equally seen in the samples with GelMA/MSN/CaPDex nanocomposites and in the osteogenic including medium, indicates the pro-

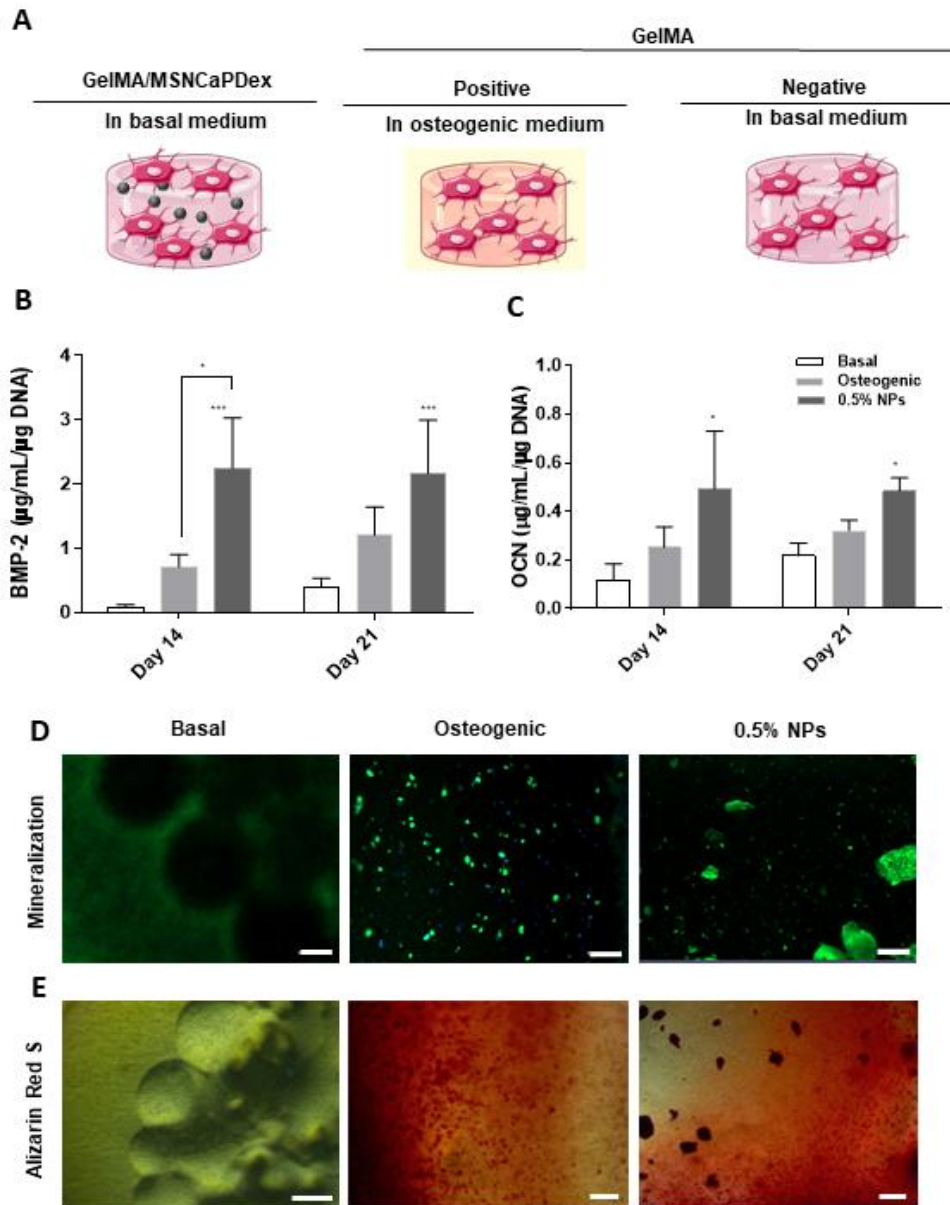


Figure 7 - (A) Evaluation of osteogenic differentiation in GelMA/MSNCaPDex nanocomposite 3D constructs incubated in basal medium and GelMA controls (positive and negative) (B) BMP-2 and (C) OCN ELISA-mediated quantification at different culture periods, namely 14 and 21 days. (D) Mineralization of hBM-MSCs obtained by OsteoImage™ staining and (E) Optical microscopy images of Alizarin Red S staining of calcium deposits produced by hBM-MSCs after 14 days in culture. Scale bars = 200 µm. Data represents mean ± s.d., n=3. *= $p < 0.05$, ***= $p < 0.001$. Symbols above bars are compared to those of basal medium.

osteogenic potential of the formulated bioink. The overall results indicate that bioactive nanoparticles presence positively influences the osteogenic differentiation of stem cells in the bioink. It is worth mentioning that differentiation studies with GelMA/MSNCaPDex were carried out using only basal medium, in order to understand the single effect of the MSNCaPDex. Opposite to most studies that use osteogenic medium [14,28,51], the goal herein is to avoid its use and rely only on biofactors released by the MSNCaPDex components present in the bioactive bioink. Through this strategy, we

prove that bioactive nanoparticles are able to bioinstruct stem cells towards osteodifferentiation in 3D bioprinted constructs in a similar mode to that of the gold standard *in vitro* method – continuous supplementation of osteogenic factors in the culture medium. To date some reports describe stem cells differentiation without the use of osteogenic supplementation using inorganic nanocarriers incorporated in hydrogels. Laponite-GelMA nanocomposite hydrogels showed to differentiate stem cells [27], while matrices of mineralized GelMA hydrogels induced the differentiation of hiPSCs [57].

Some studies have also combined the use of bioactive silicates/ calcium-deficient hydroxyapatite (CDHA) and non-porous silica nanostructures with the bioprinting technique to obtain customized nanocomposite scaffold, but some of these reports focus on the use of alginate, a rather bioinert biopolymer that is not a component of bone tissue [4,58-60]. GelMA has been used before as the main component of several bionks, and was conjugated with silica and hydroxyapatite nanoparticles to induce biomineralization [61-63], while mesoporous silica has also been combined with hydrogels to bioprint constructs to be used in bone regeneration [64,65].

In comparison to other strategies using silica/bioglass-biomaterial inks [66,67] the formulated living bioink comprising the organic-inorganic bone mimetic elements and stem cells present various advantages for bone repair because they recapitulate key bone components and also include/bioinstruct stem cells toward the osteogenic lineage. Moreover, the use of MSN/CaPDex as ions and drug depots allows the controlled release of these bioactives and the timely instruction of mesenchymal stem cells. In comparison with the inclusion of free drugs and ions in the GelMA matrix this nanocomposite-based platform circumvents the uncontrolled/swelling mediated burst release generally associated with standard hydrogel matrix [68]. Following differentiation, the presence of such bone progenitor cells is widely recognized to be advantageous owing to their ability to generate new tissue, to recruit other cells to the injured site and to establish a pro-regenerative niche via secretion of trophic factors that aid the repair process [69].

Moreover, the herein developed ink exhibits a higher complexity due to the release of several bioactive factors from the MSN mesoporous matrix, which can be functionalized to fit specific applications, further expanding its applicability. The newly formulated bioink has shown to be suitable for processing via extrusion bioprinting and the resulting biomaterial showed ability to autonomously induce osteogenic differentiation. For further studies, we hypothesize that such living constructs could maintain their bioactive and pro-osteogenic capabilities after implantation in damaged bone microenvironments. Furthermore, more complex structures can be obtained by taking advantage of the bioprinting properties. By using separate nozzles, bioinks with different components or concentrations can be bioprinted at pre-defined locations, mimicking the complexity of the bone tissue. [70-72]

4. Conclusions

In summary, herein we proposed the formulation of an intrinsically bioactive nanocomposite GelMA/MSN/CaPDex hydrogel bioink and demonstrate its potential to be used for 3D bioprinting stem cell laden constructs. The results

demonstrate the improved bioactivity and pro-osteogenic induction of these constructs in comparison to standalone GelMA bioinks cultured in basal medium and even in pro-osteogenic medium. In fact, the presence of the bioactive nanoparticles imparted nanofunctional hydrogel with efficient pro-osteochonductive properties without affecting the 3D bioprinting process. MSN/CaPDex incorporated in GelMA hydrogels have proven to induce stem cell differentiation without the need of any other osteogenic supplementation and thus they are expected to facilitate the implantation *in vivo* since they abolish the need for continuous culture in osteogenic medium. Combining this bioink printability with its inherent bioactivity, we envision that nanocomposite 3D constructs with patient-personalized sizes, tailorable mechanical properties and shapes can be fabricated, thus facilitating the implantation process. Future assays focusing on inducing biomineralization and evaluating possible immune system activation *in vivo* will further corroborate the applicability of the herein formulated nanocomposite bioink.

Acknowledgments

The authors would like to acknowledge the support of the European Research Council for project ATLAS, grant agreement ERC-2014-ADG-669858. This work was also supported by the Programa Operacional Competitividade e Internacionalização (POCI), in the component FEDER, and by national funds (OE) through FCT/MCTES, in the scope of the projects Margel (PTDC/BTM-MAT/31498/2017). M. Tavares also thanks FCT for a PhD grant (FCT-PD/BD/114019/2015). The PANGEIA project PANGEIA (PTDC/BTM-SAL/30503/2017) is also acknowledged for the junior researcher contract of Vítor Gaspar. This work was also developed within the scope of the project CICECO-Aveiro Institute of Materials, FCT Ref. UID/CTM/50011/2019, financed by national funds through the FCT/MCTES. This work was also supported by Fundos Europeus Estruturais e de Investimento (FEEI), Programa Operacional Regional de Lisboa-FEDER (02/SAICT/2017), and national funds from Fundação para a Ciência e a Tecnologia (FCT-Portugal) and COMPETE (FEDER) within projects UIDB/00100/2020 (CQE), and PTDC/CTM-CTM/32444/2017 (02/SAICT/2017/032444).

References

- [1] Lopes D L, Martins-Cruz C, Oliveira M B and Mano J F 2018 *Biomaterials* **185** 240–75
- [2] Amini A R, Laurencin C T and Nukavarapu S P 2012 *Crit. Rev. Biomed. Eng.* **40** 363–408
- [3] Kao S T and Scott D D 2007 *Oral Maxillofac. Surg. Clin. North Am.* **19** 513–21

- [4] Gao G, Schilling A F, Yonezawa T, Wang J, Dai G and Cui X 2014 *Biotechnol. J.* **9** 1304–11
- [5] Ashammakhi N, Ahadian S, Xu C, Montazerian H, Ko H, Nasiri R, Barros N and Khademhosseini A 2019 *Mater. Today Bio* **1** 100008
- [6] Aljohani W, Ullah M W, Zhang X and Yang G 2018 *Int. J. Biol. Macromol.* **107** 261–75
- [7] Chimene D, Kaunas R and Gaharwar A K 2020 *Adv. Mater.* **32** 1902026
- [8] Luz G M and Mano J F 2010 *Compos. Sci. Technol.* **70** 1777–88
- [9] Murphy S V., Skardal A and Atala A 2013 *J. Biomed. Mater. Res. - Part A* **101** 272–84
- [10] Zhang Y S and Khademhosseini A 2017 *Science (80-.)*, 356
- [11] Utech S and Boccaccini A R 2016 *J. Mater. Sci.* **51** 271–310
- [12] Xiao S, Zhao T, Wang J, Wang C, Du J, Ying L, Lin J, Zhang C, Hu W, Wang L and Xu K 2019 *Stem Cell Rev. Reports* **15** 664–79
- [13] Aldana A A, Malatto L, Ur Rehman M A, Boccaccini A R and Abraham G A 2019 *Nanomaterials* **9** 120
- [14] Lee D, Choi E J, Lee S E, Kang K L, Moon H J, Kim H J, Youn Y H, Heo D N, Lee S J, Nah H, Hwang Y S, Lee Y H, Seong J, Do S H and Kwon I K 2019 *Chem. Eng. J.* **365** 30–9
- [15] Schuurman W, Levett P A, Pot M W, Weeren V, Dhert W J A, Hutmacher D W, Melchels F P W, Klein T J and Malda J 2013 *Biosci.* **13** 551–61
- [16] Monteiro M V, Gaspar V M, Ferreira L P and Mano J F 2020 *Biomater. Sci.* **8** 1855–64
- [17] Antunes J, Gaspar V M, Ferreira L, Monteiro M, Henrique R, Jerónimo C and Mano J F 2019 *Acta Biomater.* **94** 392–409
- [18] Shin S R, Zihlmann C, Akbari M, Assawes P, Cheung L, Zhang K, Manoharan V, Zhang Y S, Yükksekaya M, Wan K T, Nikkhah M, Dokmeci M R, Tang X S and Khademhosseini A 2016 *Small* **12** 3677–89
- [19] Ebrahimi M, Ostrovidov S, Salehi S, Kim S B, Bae H and Khademhosseini A 2018 *J. Tissue Eng. Regen. Med.* **12** 2151–63
- [20] Gan D, Xu T, Xing W, Wang M, Fang J, Wang K, Ge X, Chan C W, Ren F, Tan H and Lu X 2019 *J. Mater. Chem. B* **7** 1716–25
- [21] Liu W, Zhong Z, Hu N, Zhou Y, Maggio L, Miri A K, Fragasso A, Jin X, Khademhosseini A and Zhang Y S 2018 *Biofabrication* **10** 024102
- [22] Yin J, Yan M, Wang Y, Fu J and Suo H 2018 *ACS Appl. Mater. Interfaces* **10** 6849–57
- [23] Bertassoni L E, Cardoso J C, Manoharan V, Cristino A L, Bhise N S, Araujo W A, Zorlutuna P, Vrana N E, Ghaemmaghami A M, Dokmeci M R and Khademhosseini A 2014 *Biofabrication* **6** 024105
- [24] Liu W, Heinrich M A, Zhou Y, Akpek A, Hu N, Liu X, Guan X, Zhong Z, Jin X, Khademhosseini A and Zhang Y S 2017 *Adv. Healthc. Mater.* **6** 1601451
- [25] Lavrador P L, Esteves M, Gaspar V M and Mano J F *Adv. Funct. Mater.* 2020, doi.org/10.1002/adfm.202005941
- [26] Leite A J, Oliveira M B, Caridade S G and Mano J F 2017 *Adv. Funct. Mater.* **27** 1701219
- [27] Xavier J R, Thakur T, Desai P, Jaiswal M K, Sears N, Cosgriff-hernandez E, Kaunas R, Gaharwar A K and Al X E T 2015 *ACS Nano* **9** 3109–18
- [28] Paul A, Manoharan V, Krafft D, Assmann A, Uquillas J A, Shin S R, Hasan A, Hussain M A, Memic A, Gaharwar A K and Khademhosseini A 2016 *J. Mater. Chem. B* **4** 3544–54
- [29] Tavares M T, Oliveira M B, Mano J F, Farinha J P S and Baleizão C 2020 *Mater. Sci. Eng. C* **107** 110348
- [30] Leite Á J, Sarker B, Zehnder T, Silva R, Mano J F and Boccaccini A R 2016 *Biofabrication* **8** 035005
- [31] Zhang Q, Qin M, Zhou X, Nie W, Wang W, Li L and He C 2018 *J. Mater. Chem. B* **6** 6731–43
- [32] Baleizão C and Farinha J P S 2015 *Nanomedicine* **10** 1–7
- [33] Bonjour J P 2011 *J. Am. Coll. Nutr.* **30** 438S-448S
- [34] Min Z, Huixue W, Yujie Z, Lixin J, Hai H and Yufang Z 2016 *Mater. Lett.* **171** 259–62
- [35] Langenbach F and Handschel J 2013 *Stem Cell Res. Ther.* **4** 1
- [36] Cholkar K, Hariharan S, Gunda S and Mitra A K 2014 *AAPS PharmSciTech* **15** 1454–67
- [37] Tavares M T, Oliveira M B, Gaspar V M, Mano J F, Farinha J P S and Baleizão C 2020 *Adv. Biosyst.* 10.1002/adbi.202000123.
- [38] Ribeiro T, Coutinho E, Rodrigues A S, Baleizão C and Farinha J P S 2017 *Nanoscale* **9** 13485–94
- [39] Lin Y, Tsai C, Huang H, Kuo C, Hung Y, Huang D, Chen Y and Mou C 2005 *Chem Mater* **17** 4570
- [40] Ribeiro T, Rodrigues A S, Calderon S, Fidalgo A, Gonçalves J L M, André V, Teresa Duarte M, Ferreira P J, Farinha J P S and Baleizão C 2020 *J. Colloid Interface Sci.* **561** 609–19
- [41] Ribeiro, A., Blokzijl, M. M., Levato, R., Visser, C. W., Castilho, M., Hennink, W. E., Malda, J. 2017 *Biofabrication*, 10, 014102.
- [42] Kokubo T, Kushitani H, Sakka S, Kitsugi T and Yamamuro T 1990 *J. Biomed. Mater. Res.* **24** 721–34
- [43] JB V 2019 *Photocrosslinking Optimization Protocol CELLINK 3*
- [44] Kumari S, Bargel H, Scheibel T 2019 *Macromolecular Rapid Communications* **41** 1
- [45] Zhou X, Zhang N, Mankoci S and Sahai N 2017 *J. Biomed. Mater. Res. - Part A* **105** 2090–102
- [46] Jones J R 2015 *Acta Biomater.* **23** S53–82

- [47] Raynaud S, Champion E, Bernache-Assollant D, Laval JP 2001 *J Am. Ceram. Soc.* **84** 359-66
- [48] Leite Á J, Oliveira N M, Song W and Mano J F 2018 *Sci. Rep.* **8** 1–11
- [49] Luz G M and Mano J F 2011 *Nanotechnology* **22** 494014
- [50] Shao N, Guo J, Guan Y, Zhang H, Li X, Chen X, Zhou D and Huang Y 2018 *Biomacromolecules* **19** 3637–48
- [51] Kwon S, Lee S S, Sivashanmugam A, Kwon J, Kim S H L, Noh M Y, Kwon S K, Jayakumar R and Hwang N S 2018 *Polymers (Basel)*. **10** 914
- [52] Lavrador P, Gaspar V M and Mano J F 2018 *Adv. Healthc. Mater.* **8** 1800890
- [53] Celikkin N, Mastrogiacomo S, Jaroszewicz J, Walboomers X F and Swieszkowski W 2018 *J. Biomed. Mater. Res. - Part A* **106** 201–9
- [54] Du M, Chen B, Meng Q, Liu S, Zheng X, Zhang C, Wang H, Li H, Wang N and Dai J 2015 *Biofabrication* **7** 44104
- [55] Zhu W, Cui H, Boualam B, Masood F, Flynn E, Rao R D, Zhang Z Y and Zhang L G 2018 *Nanotechnology* **29** 185101
- [56] Patricia Ducy, Desbois C, Boyce B, Pinero G, Story B, Dunstan C, Smith E, Bonadio J, Godlstein S, Gundberg C, Bradley A and Karsenty G 1996 *Nature* **382** 448–52
- [57] Kang H, Shih Y V, Hwang Y, Wen C, Rao V, Seo T and Varghese S 2014 *Acta Biomater.* **10** 4961–70
- [58] Wang X, Tolba E, Der H C S, Neufurth M, Feng Q, Diehl-Seifert B R and Müller W E G 2014 *PLoS One* **9** 1–7
- [59] Raja N, Yun, H 2016 *J. Mater. Chem. B* **4** 4707-4716
- [60] Ojansivu M, Rashad A, Ahlinder A, Massera J, Mishra A, Syverud K, Finne-Wistrand A, Miettinen S and Mustafa K 2019 *Biofabrication* **11** 035010
- [61] Byambaa B, Annabi N, Yue K, Trujillo-de Santiago G, Alvarez M M, Jia W, Kazemzadeh-Narbat M, Shin S R, Tamayol A and Khademhosseini A 2017 *Adv. Healthc. Mater.* **6** 1700015
- [62] Sadat-Shojai M, Khorasani M T and Jamshidi A 2015 *Mater. Sci. Eng. C* **49** 835–43
- [63] Nowicki M A, Castro N J, Plesniak M W and Zhang L G 2016 *Nanotechnology* **27** 414001
- [64] Min Z, Kun L, Yufang Z, Jianhua Z and Xiaojian Y 2015 *Acta Biomater.* **16** 145–55
- [65] Li K, Zhu M, Xu P, Xi Y, Cheng Z, Zhu Y and Ye X 2015 *J. Mater. Sci. Mater. Med.* **26** 102
- [66] Paxton NCP, Ren J, Ainsworth MJ, Solanki AK, Jones JR, Allenby MC, Stevens MM, Woodruff MA 2019 *Macrom Rapid Comm* **40** 11
- [67] Richter RF, Ahlfeld T, Gelinsky M, Lode A 2019 *Materials* **12** 2022
- [68] Li J, Mooney DJ 2016 *Nat Rev Mater* **1** 16071
- [69] Lin H, Sohn J, Shen H, Langhans MT, Tuan RS 2019 *Biomaterials* **203** 96-110
- [70] Gardan J 2019 *Virtual Phys Prototyp.* **14** 1
- [71] Lee JM, Swee LS, Wai, YY 2020 *Int. J Bioprint.* **6** 1
- [72] Feng F, He J, Li J 2019 *Int J Bioprint.* **5** 2